

Spherical Actuation Using the Displaced Trapezoidal Winding *

Lyndon Scott Stephens
 Bearings and Seals Laboratory
 University of Kentucky
 Lexington, KY 40506, USA
 stephens@engr.uky.edu

David J. Carroll
 Engineering
 Airex Corporation
 Somersworth, NH 03878, USA
 dcarroll@airex.com

Abstract – Previous work has shown that the segmented displaced trapezoidal winding produces Lorentz forces in two orthogonal directions on a permanent magnet rotor. This paper presents a unique collection of trapezoidal windings in a spherical geometry to provide active control of all 6 degrees of freedom. Equations for force and torque generation are presented, and a “decoupling” control scheme is applied to the actuator such that the 3 bearing forces and 3 control torques are decoupled and independent. The construction of a prototype is also discussed and experimental results are presented with good agreement with the theory.

Index Terms – Self Bearing Motor, Bearingless Motor, Spherical Actuator, Lorentz Force Actuator

I. INTRODUCTION

In previous work [1], the segmented displaced trapezoidal winding (SDTW) was introduced for force and torque production in a cylindrical actuator geometry to form a self bearing motor with support in 2 radial degrees of freedom and one rotational degree of freedom. As Figure 1 illustrates, two windings with opposite skew angle directions, α , are arranged one on top of another to form an “x” pattern. Using this patented arrangement [2], Lorentz forces are generated on a set of permanent magnets, producing bi-directional control forces in two orthogonal directions per the following schedule:

Table I
Trapezoidal Winding Actuation Summary

$\text{Sgn}(i_{11})$	$\text{Sgn}(i_{13})$	Actuation
>0	>0	+ θ
<0	<0	- θ
<0	>0	+z
>0	<0	-z

The trapezoidal winding is a distributed winding sheet consisting of only a few strands of wire in thickness such that it is pliable and can be “molded” around a given geometry. This paper describes the application of the trapezoidal winding onto a spherical, slotless back iron, geometry to produce 6 DOF active force and torque

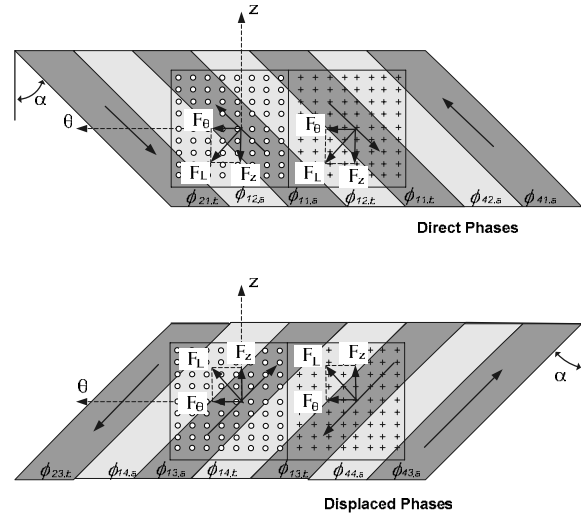


Figure 1: Force Generation in Segmented Trapezoidal Windings

generation. The slotless construction results in smooth angular rotation by eliminating detent and cogging torque. Equations for 6 DOF control and for force and torque production are presented. The construction of a small (<29 mm diameter) prototype is also discussed. The technology is directly applicable to a MINI-CD ROM, but may be applied to other small machines.

II. PROTOTYPE CONSTRUCTION

Figure 2 shows a schematic of the 29 mm diameter spherical prototype. The rotor is comprised of a mating pair of cylindrical cobalt iron sleeves, each internally tiled with alternating polarity permanent magnet arc segments that form the hemispherical inside surface as seen in Figure 3. When mated, the rotor sleeves are positioned to align magnet poles of the same polarity. The spherical stator is unique in that the copper conductors are machine wound directly over the epoxy insulated powdered iron core. Aluminum mandrels were used to attach the core to the winding machine and steel pins were axially inserted into pre-machined holes to capture and hold the winding end-turns until the coils are secured with tape as seen in Figure 4. Once the winding process was complete, the pins were removed and the coils were formed using two heated

* This work is partially supported by the United States Air Force under contract number 29601-01-C-0174.

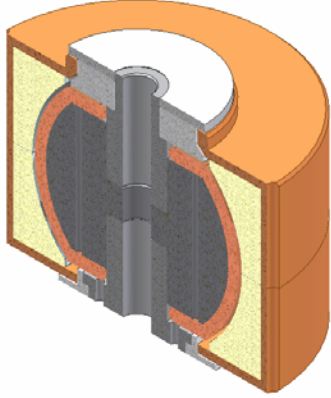


Figure 2: Spherical Motor Diagram

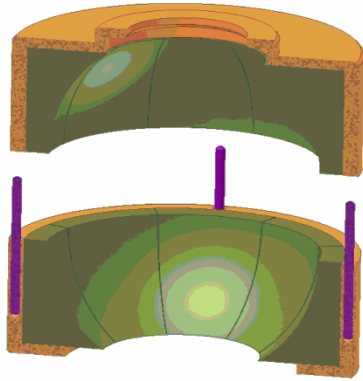


Figure 3: Spherical Rotor Diagram

hemispherical cavities pressed around the coils. The heat activates and fuses the bondable coating on the surface of each wire to neighbouring conductors thus bonding the wire entire winding into a solid spherical shape. The bondable coating also adheres to the epoxy insulated core thus solidly anchoring the winding to the supporting structure.

The aluminum mandrels were removed and a single long screw was used to mount the stator to a PC board. The stator back-iron incorporates features required to stand the core away from the PC board mounting surface leaving room for the lead wires to exit while simultaneously clamping plastic rings in place to act as a backup bearing for the system. The bonded stator assembly and half of the rotor can be seen in Figure 5.

The stator core profile is formed by using off-center radii that directly compensate for the increasing winding thickness with increasing latitude such that the clearance gap between the outer surface of the winding and the rotor is maintained as a uniform thickness spherical shell. At the stator “equator”, the slots are shallow and relatively wide,



Figure 4: Stator Windings Before Forming

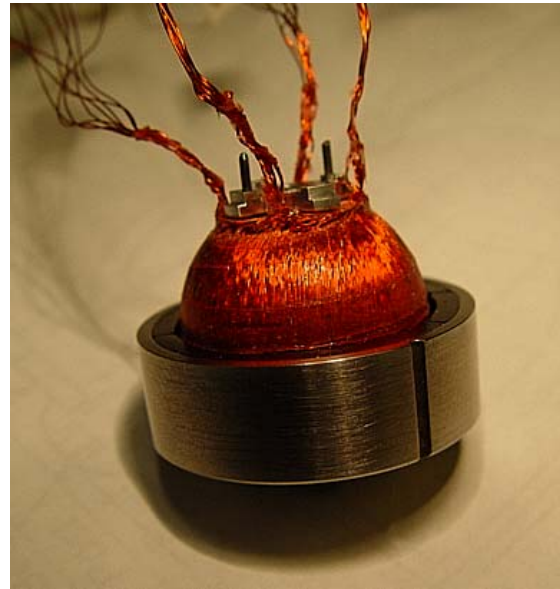


Figure 5: Formed Stator Winding and PM Rotor Half

however, at the higher latitudes the slots deepen as they narrow to maintain the same cross sectional slot area for the windings. The cylindrical outer shape of the rotor provides increasing magnet thickness with increasing latitude and thus helps maintain the flux levels despite the increase in magnetic gap.

III. FORCE AND TORQUE GENERATION

Figure 6 shows a cut-away view of a generic trapezoidal winding spherical actuator (with PM magnets on the ID instead of the outside of the stator) at the mid-plane looking downward onto the actuator. As the figure shows, the windings are arranged into 4 segments with 4 windings in each segment. With this arrangement, independent surface forces are generated on the rotor by each segment. By simultaneously modulating the current (forces) in opposing segments, control forces F_x and F_y are generated, along with the torque about the about the z-axis, T_z . The z-direction force, F_z , and the torques about the x and y axes

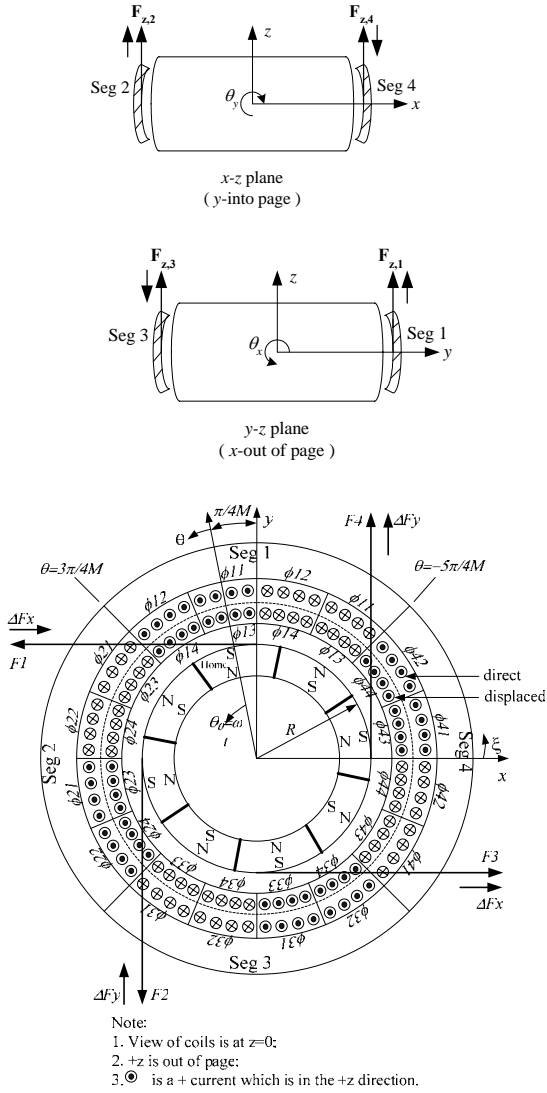


Figure 6: Force and Torque Production Note: Drawn as an inside rotor system – if magnets were on the outside their polarity would need to be inverted

are generated using the differential skew angle of the direct and displaced coils in a given segment (previously shown in Figure 1) and by modulating these forces in opposing segments. Figure 6 also shows cut-away views in the x-z and y-z planes.

Control of each of the 6 DOF is first evaluated using 6 control currents, $\mathbf{i}_c = [i_x, i_y, i_z, i_{\theta_x}, i_{\theta_y}, i_{\theta_z}]^T$ and distributing them into the stator winding currents, \mathbf{i}_s , using the following physically motivated 8x6 mapping matrix, W .

$$\mathbf{i}_s = \begin{bmatrix} i_{1,direct} \\ i_{1,displ} \\ i_{2,direct} \\ i_{2,displ} \\ i_{3,direct} \\ i_{3,displ} \\ i_{4,direct} \\ i_{4,displ} \end{bmatrix} = \underbrace{\begin{bmatrix} -1 & 0 & 1 & 1 & 0 & 1 \\ -1 & 0 & -1 & -1 & 0 & 1 \\ 0 & -1 & 1 & 0 & 1 & 1 \\ 0 & -1 & -1 & 0 & -1 & 1 \\ 1 & 0 & 1 & -1 & 0 & 1 \\ 1 & 0 & -1 & 1 & 0 & 1 \\ 0 & 1 & 1 & 0 & -1 & 1 \\ 0 & 1 & -1 & 0 & 1 & 1 \end{bmatrix}}_W \begin{bmatrix} i_x \\ i_y \\ i_z \\ i_{\theta_x} \\ i_{\theta_y} \\ i_{\theta_z} \end{bmatrix} \quad (1)$$

Assuming that this actuator acts as a bearing in the x, y, z, θ_x , and θ_y degrees of freedom (small displacements) and provides motoring about the θ_z axis (large displacement), then based on the rotor home position shown in Figure 6, the symmetric commutation mapping equations are:

$$\mathbf{i}_\phi = \underbrace{\begin{bmatrix} H & 0_{4 \times 2} & 0_{4 \times 2} & 0_{4 \times 2} \\ 0_{4 \times 2} & H & 0_{4 \times 2} & 0_{4 \times 2} \\ 0_{4 \times 2} & 0_{4 \times 2} & H & 0_{4 \times 2} \\ 0_{4 \times 2} & 0_{4 \times 2} & 0_{4 \times 2} & H \end{bmatrix}}_Y \mathbf{i}_s \quad (2)$$

where $\mathbf{i}_\phi = [i_{11}, i_{12}, i_{13}, i_{14}, i_{21}, \dots, i_{44}]^T$ is the vector of phase currents corresponding to Figure 6 and Y is the 16x8 commutation mapping matrix in which the 4x2 matrix, H is:

$$H = \begin{bmatrix} \cos \left[M \left(\theta_z - \frac{\pi}{16} \right) - \gamma \right] & 0 \\ \cos \left[M \left(\theta_z - \frac{\pi}{16} \right) - \gamma - \frac{\pi}{2} \right] & 0 \\ 0 & \cos \left[M \left(\theta_z - \frac{\pi}{16} \right) - \gamma \right] \\ 0 & \cos \left[M \left(\theta_z - \frac{\pi}{16} \right) - \gamma - \frac{\pi}{2} \right] \end{bmatrix} \quad (3)$$

where M is the number of permanent magnet pole pairs and γ is the phase lag or lead depending on the skew angle of the particular phase between the angular motion, θ_z , and the phase current, $i_{k,j}$. This term can be neglected for this design because small displacements in the z direction are assumed.

Force and torque computations are accomplished using the following coordinate systems:

- **Frame n:** $[\mathbf{n}_1, \mathbf{n}_2, \mathbf{n}_3]$ global Cartesian reference frame in line with x, y and z axes in Figure 6
- **Frame a:** $[\mathbf{a}_1, \mathbf{a}_2, \mathbf{a}_3]$ slot Cartesian reference frame in line with the center of a given slot on the

equator of the sphere. Simple rotation about \mathbf{n}_3 by angle ψ .

- **Frame \mathbf{b} :** $[\mathbf{b}_1, \mathbf{b}_2, \mathbf{b}_3]$ slot Cartesian reference frame in line with a given skewed coil. Simple rotation about \mathbf{a}_1 by the skew angle, α .
- **Frame \mathbf{S}_1 :** $[\mathbf{r}_1, \theta_1, \phi_1]$ slot spherical reference frame with respect to reference frame \mathbf{b} .
- **Frame \mathbf{c} :** $[\mathbf{c}_1, \mathbf{c}_2, \mathbf{c}_3]$ rotating Cartesian reference frame embedded in the rotor. Simple rotation about \mathbf{n}_3 by the angle $\theta_z + \pi/16$.
- **Frame \mathbf{S}_2 :** $[\mathbf{r}_2, \theta_2, \phi_2]$ rotor spherical reference frame with respect to reference frame \mathbf{c} .

Conversions between each of these reference frames are accomplished using simple Euler angle and spherical coordinate transformations which are well documented elsewhere. The phase currents of equation (2) are distributed into the appropriate slots of the actuator as shown in Figure 6. This results in a total of 32 current sheets (16 direct and 16 displaced) that comprise the stator. These current sheets are numbered beginning with $n=1$ for phase ϕ_{41} and continuing CCW such that $n=16$ for phase ϕ_{42} , $n=17$ for phase ϕ_{43} and $n=32$ for phase ϕ_{44} . The total current per unit latitude at the equator in a given sheet is given in spherical reference frame \mathbf{S}_1 as:

$$\mathbf{I}_n = \begin{cases} \frac{N}{r_o(\pi/8)} i_n \boldsymbol{\phi}_1 & r = r_o, \quad -\frac{\pi}{16} < \theta_1 < \frac{\pi}{16}, \quad 0 < \phi_1 < \pi \\ 0 & \text{otherwise} \end{cases} \quad (4)$$

where, N is the number of conductors per slot, i_n is the current in the n^{th} ($n=1$ to 32) current sheet and r_o is the rotor inner radius. The slot total current vector is then constructed as:

$$\mathbf{i}_{st} = \left[\begin{array}{c|c} \text{direct phases} & \text{displaced phases} \\ \hline \mathbf{I}_1 & \mathbf{I}_{17} \\ \mathbf{I}_2 & \mathbf{I}_{18} \\ \cdots & \cdots \\ \mathbf{I}_{16} & \mathbf{I}_{32} \end{array} \right]^T \quad (5)$$

and is related to the phase current vector by the phase distribution matrix, Λ :

$$\mathbf{i}_{st} = \frac{N}{r_o \frac{\pi}{8}} \boldsymbol{\phi}_1 \underbrace{\begin{bmatrix} d_3 & 0 & 0 & d_1 \\ d_1 & d_3 & 0 & 0 \\ 0 & d_1 & d_3 & 0 \\ 0 & 0 & d_1 & d_3 \\ d_2 & 0 & 0 & d_4 \\ d_4 & d_2 & 0 & 0 \\ 0 & d_4 & d_2 & 0 \\ 0 & 0 & d_4 & d_2 \end{bmatrix}}_{\Lambda} \mathbf{i}_{\phi} \quad (6)$$

where,

$$d_1 = \begin{bmatrix} 1 & 0 & 0 & 0 \\ 0 & 1 & 0 & 0 \\ 0 & 0 & 0 & 0 \\ 0 & 0 & 0 & 0 \end{bmatrix} \quad d_2 = \begin{bmatrix} 0 & 0 & 0 & 0 \\ 0 & 0 & 0 & 0 \\ 0 & 0 & -1 & 0 \\ 0 & 0 & 0 & -1 \end{bmatrix} \quad (7)$$

$$d_4 = \begin{bmatrix} 0 & 0 & 1 & 0 \\ 0 & 0 & 0 & 1 \\ 0 & 0 & 0 & 0 \\ 0 & 0 & 0 & 0 \end{bmatrix} \quad d_3 = \begin{bmatrix} 0 & 0 & 0 & 0 \\ 0 & 0 & 0 & 0 \\ -1 & 0 & 0 & 0 \\ 0 & -1 & 0 & 0 \end{bmatrix}$$

The flux density due to the permanent magnets is defined in spherical reference frame \mathbf{S}_2 as:

$$\mathbf{B}_m = \begin{cases} (-1)^m B_{pm} \mathbf{r}_2 & r_2 = r_o, \quad \beta < \phi_2 < \pi - \beta, \\ -\frac{\pi}{8} + (m-1)\frac{\pi}{4} < \theta_2 < \frac{\pi}{8} + (m-1)\frac{\pi}{4} \\ 0 & \text{otherwise} \end{cases} \quad (8)$$

where B_{pm} is the permanent magnet flux density magnitude, which is assumed to be constant across the pole for the purposes of this paper, and m indicates the specific permanent magnet under consideration around the circumference of the rotor ($m=1$ to 8). In this definition, $m=1$ corresponds to the permanent magnet that is intersected by the coordinate, \mathbf{c}_1 , embedded in the rotor. Subsequent PM segments are numbered sequentially in a CCW fashion around the equator of the rotor looking downward as in Figure 6.

Computation of the force and torque on the rotor is accomplished by discretizing the spherical domain into discrete points and computing the control force vector, $\mathbf{F}_c = [F_x, F_y, F_z, T_x, T_y, T_z]^T$ as:

$$\mathbf{F}_c = \underbrace{\begin{bmatrix} \mathbf{F}_{n=1} & \mathbf{F}_{n=2} & \cdots & \mathbf{F}_{n=32} \\ \mathbf{T}_{n=1} & \mathbf{T}_{n=2} & \cdots & \mathbf{T}_{n=32} \end{bmatrix}}_{\Phi} \mathbf{i}_{st} \quad (9)$$

where Φ is the flux linkage matrix and $\mathbf{F}_n = [F_x, F_y, F_z]^T$ at the n^{th} slot and $\mathbf{T}_n = [T_x, T_y, T_z]^T$ at the n^{th} slot. Each element of Φ is then computed as:

$$\mathbf{F}_n = \left(\sum \underbrace{\mathbf{B}_i \times \mathbf{I}_i}_{\mathbf{f}_i} \frac{1}{|\mathbf{I}_i|} \right) \Delta L_{\phi} \Delta L_{\theta} \quad (10)$$

$$\mathbf{T}_n = \sum \mathbf{P}_i \times \left(\underbrace{\mathbf{B}_i \times \mathbf{I}_i}_{\mathbf{f}_i} \right) \frac{1}{|\mathbf{I}_i|} \Delta L_{\phi} \Delta L_{\theta}$$

where \mathbf{F}_n is the force per unit current due to the n^{th} current sheet, ΔL_{ϕ} and ΔL_{θ} are the discretization lengths in the latitudinal and longitudinal directions, and \mathbf{P}_i is the position vector from the center of the sphere to any point on the line of action of the i^{th} discrete actuator force, \mathbf{f}_i .

IV. DECOUPLING CONTROL

The current mapping matrix, W , in equation (1) is physically motivated by the layout of the spherical actuator. As will be seen in the results section that follows, the use of W results in cross-coupled current gains. It is desired to decouple the actuator by defining a different mapping matrix. The approach presented in [3] gives the general result for decoupling control of pure Lorentz force actuators and is applicable to the spherical actuator. The objective of decoupling control is to find W such that independent control forces in all 6 degrees of freedom are generated at all angular motoring positions, θ_z . According to [3], any arbitrary actuator current gain matrix, K_i , is achievable under the following mapping:

$$W = A^+ K_i \quad (11)$$

where $A^+ = A^T(AA^T)^{-1}$ and is the Moore-Penrose pseudo-inverse of the underdetermined model, $A = \Phi \Lambda Y$, as long as the pseudo-inverse exists. The test for existence indicates that the actuator can be decoupled as long as:

$$|AA^T| \neq 0 \quad \forall \theta_z \quad (12)$$

V. RESULTS

For the spherical actuator prototype the rotor inner diameter is $r_o = 11.125$ mm, there are 25 turns of 30 AWG wire per winding with two windings per slot, the calculated flux density is $B_{pm} = 0.73$ T, the actual average skew angle is $\alpha = 10.4^\circ$ and the PM rotor angle is $\beta = 42.4^\circ$. These numbers were used in equations (1)-(10) to generate force and torque curves versus angular rotation over one permanent magnet pole pitch. Note that this case corresponds to the physically motivated current mapping, W , which is not decoupled necessarily. Figure 7 shows the bearing forces for a control current of $i_z = 1.0$, and all other control currents zero. The average force in the z-direction is 1.1 N for the actuator and independent bearing forces and torques are generated. Figure 8 shows the motoring torque for a control current of $i_{\theta_z} = 1.0$ A. Note that in both cases there is a slight ripple in the force and torque production versus rotor angle, θ_z .

Figure 9 shows the x and y direction forces that result for a control current of $i_x = 1.0$. Similarly, Figure 10 shows the θ_x and θ_y direction torques that result for a control current of $i_{\theta_x} = 1.0$ A. These curves indicate that in addition to the ripple in the force and torque production there is a cross-coupling in the x and y directions for this actuator under the current control mapping defined in equation (1). Note that at certain rotor angles the cross coupling is degenerate to zero, but at other rotor angles it is 15-20% of the direct forces. The cross-coupling is brought about by the layout of the actuator and could be reduced via an increased number of poles or by use of asymmetrical commutation. The approach taken here is to use the decoupling control of equation (11). Using the

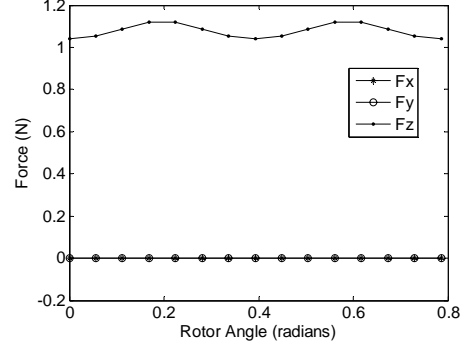


Figure 7: Bearing Force for $i_z = 1.0$ A

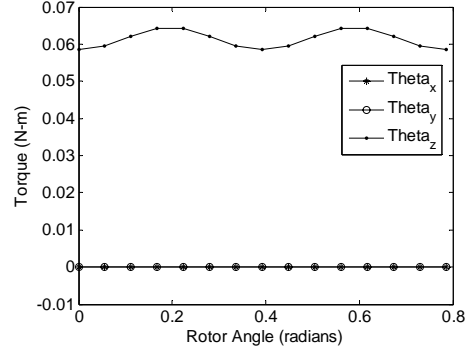


Figure 8: Motor Torque for $i_{\theta_z} = 1.0$ A

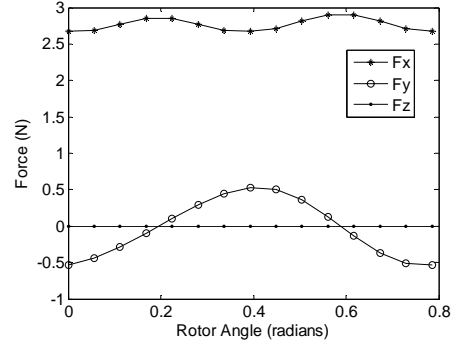


Figure 9: Bearing Force for $i_x = 1.0$ A

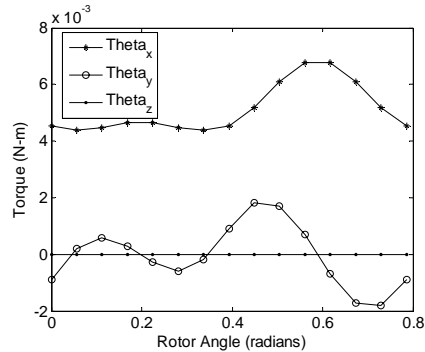


Figure 10: Motor Torque for $i_{\theta_x} = 1.0$ A

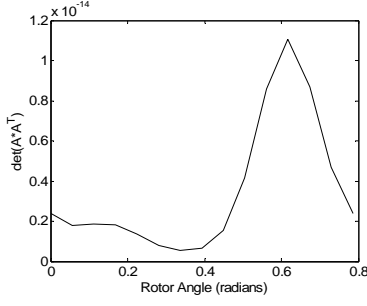


Figure 11: Test Parameter for Existence Of Decoupling Control

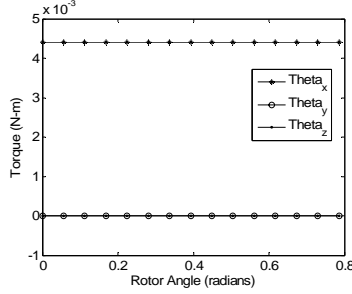


Figure 12: Motor Torque for $i_{\theta_x}=1.0$ A under decoupling control

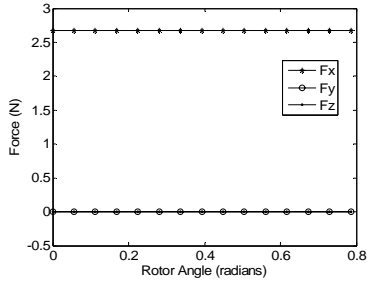


Figure 13: Motor Force for $i_{\theta_x}=1.0$ A under decoupling control

previous results, the direct current gains are arranged in the desired current gain matrix as follows:

$$K_i = \begin{bmatrix} 2.6 & 0 & 0 & 0 & 0 & 0 \\ 0 & 2.6 & 0 & 0 & 0 & 0 \\ 0 & 0 & 1.1 & 0 & 0 & 0 \\ 0 & 0 & 0 & 0.0044 & 0 & 0 \\ 0 & 0 & 0 & 0 & 0.0044 & 0 \\ 0 & 0 & 0 & 0 & 0 & 0.06 \end{bmatrix} \quad (12)$$

For comparison, this desired current gain matrix is used in the decoupling control algorithm to generate similar results. The first question is whether a control mapping, W , exists that can decouple the actuator at all rotor angles. Figure 11 shows the results of the existence test defined in equation (12). In this case, the test parameter is quite small at all rotor angles, but is not zero at any one, therefore, the actuator can be decoupled using this approach. Figure 12 shows the θ_x and θ_y direction torques

that result for a control current of $i_{\theta_x} = 1.0$ A. Figure 13 shows the x and y direction forces that result for a control current of $i_x=1.0$. Note that the torque ripple and the cross-coupling have been removed from the system.

VI. DISCUSSION

The various current gains and effective winding skew angle were determined by analysis of measured back emf. To facilitate the generated voltage and phase measurement over the necessary range of radial and axial positions, the spherical actuator prototype was mounted in a milling machine capable of spinning the PM rotor while holding the stator at various X, Y, and Z positions. The experimental results showed a z-direction force current gain of 0.145 N/Amp and an average torque current gain of 0.009 N-m/Amp. The average back emf constant was found to be 0.94 volts/1000 rpm which equates to a “no-loss” torque constant of 0.009 N-m/A. The resulting measured skew angle varied from phase to phase and maintained an average of 10.4 degrees. This is compared to a z-direction force current gain of 0.10 N/Amp and a torque current gain of 0.56 N-m/Amp computed using the theoretical model. The difference between the experiment and theory is probably due to the variation in the construction of the actuator in terms of the skew angle and the number of turns varying from phase to phase. Finally, additional tests indicate a relatively low phase inductance of 120 μ H and a phase resistance of 3.2 Ω . The current gain for the control torques is seen to be quite low at 4.4 N-mm/Ampere for θ_x and θ_y , and 60.0 N-mm/Ampere for θ_z . This is due to the low skew angle of 10.4 degrees that resulted after winding. A larger skew angle would trade off the θ_z drive torque with the θ_x and θ_y torques. The maximum design current is 1.0 Amperes indicating a peak bearing force of 2.6 N and a peak torque of 60 N-mm.

VII. CONCLUSIONS

This paper presented a new type of spherical actuator that uses a collection of segmented trapezoidal windings to produce active control in 6 degrees of freedom. Agreement was seen between experimental and theoretical force and torque production. Actuator control using a physically motivated current mapping and symmetric commutation sequence resulted in cross-coupling in the x and y directions. The actuator was decoupled using a model based control method that inverts the system model onto itself.

REFERENCES

- [1] Stephens, L.S. and Impellizzeri, D., “Analysis of the Segmented Displaced Trapezoidal Winding for Force and Torque Production As a Self Bearing Motor”, ASME IGTI Paper No. GT-2005-68076.
- [2] Carroll, D.J. and Salwen, J.D., “Magnetic Bearings Using Displacement Winding Techniques”, US Patent Application No. S/N 11/125,917.
- [3] Stephens, L.S. and Ranganathan, A., “Fault Tolerant Control of a Lorentz Self Bearing Motor Considering Open Coil Faults”, Proceedings of the 9th International Symposium on Magnetic Bearings, August, 2004, Lexington, Kentucky